Supporting Information

Herling et al. 10.1073/pnas.1417326112

Spherulite Growth Kinetics

The growth rates of insulin spherulites and the bending rate of the PDMS microcantilevers were measured through time-resolved imaging of the microfluidic devices during the stall point experiments (Fig. 1). Videos of these time courses can be seen in Movies S1–S5, and individual images are shown in Fig. 2*A*. If the flow of insulin monomer was stopped, the spherulites would cease to grow, as can be seen in Movie S6. After incubation and growth within the microfluidic devices, the spherulites maintained the Maltese cross polarization pattern, when placed between cross polarizers and a wave plate at 90° (Fig. S1*B*), and the polarization pattern characteristic of radially arranged fibrils, when the wave plate was positioned at 45° (Fig. S1*D*).

The rates of spherulite growth and cantilever deflection were found by measuring the positions of the spherulite and wall edges for the acquired time course images using software written in Python, the growth and deflection rates were found as the slope of the edge position against time (Fig. S1*A*). The measured rates of spherulite growth are similar for all five cantilever geometries with an average of 0.21 ± 0.06 μm·min^{-1}. For the three values of t where a stall point was observed, the rate of spherulite growth in the presence of an opposing force was reduced to 32 ± 3% of the growth rate into free solution (Fig. 1). The lower fibril growth rate against the cantilever face, resulting in the rate of deflection, could be due to a combination of the opposing pressure and the spherulite/cantilever interface being less accessible to monomer from solution. The similar rates of spherulite growth also show that the supply of monomer through infusion by a syringe pump was kept constant between experiments.

Materials Testing of PDMS

The properties of the PDMS devices used in the microcantilever experiments were characterized in terms of the hyperelastic stress–strain behavior and viscoelastic behavior of the material. The stress–strain behavior was measured through bulk compression tests using a custom-built setup, depicted in Fig. S2*A*. The loads were applied incrementally using static weights. Displacements were measured using a scanning laser with a resolution of 3 μm. The stress–strain curve is shown in Fig. S2*B*. The response is nonlinear, but (hyper)elastic nonetheless.

The viscoelastic properties were measured using a conventional stress relaxation test. A specimen of PDMS (area = 112 mm^2) was compressed between flat platens of hardened steel using a Tinius Olsen mechanical test machine with a 500-N load cell. The imposed strain was 25%. The rise time was 1.6 s. The load on the specimen was recorded throughout the duration of the test. The stress relaxation behavior is shown in Fig. S2*C*. Using these data, and a Poisson's ratio of 0.49, the shear relaxation modulus was calculated. The shear relaxation modulus, normalized by the instantaneous shear modulus (0.54 MPa), is shown in Fig. S2*D*.

Stall Force

For each value of t, the measured stall force was scaled by the Boltzmann constant, k_B, absolute temperature T, and the average polymer length, pl, to give the force in dimensionless terms (see Fig. S3).

From the measured stall force, F, we were able to estimate the free energy associated with monomer addition to the growing fibrils (1):

$$F\,l = k_B T \ln \frac{c}{c_c}, \qquad \text{[S1]}$$

where c is the monomer concentration, $c^\circ = 1$ M, the standard concentration, and the critical concentration, $c_c = k_{off}/k_{on}$, and thereby the equilibrium dissociation constant (2). In this calculation, we have used the size of monomeric insulin as the step length, l (3). For a given monomer concentration, ΔG_r for monomer addition in the presence of a force is given by the following:

$$\Delta G_r = \Delta G_r^\circ - k_B T \ln \frac{c}{c^\circ} + F\,l. \qquad \text{[S2]}$$

At the stall point, $\Delta G_r = 0$, and thus,

$$\Delta G_r^\circ = RT \ln \frac{c}{c^\circ} - F\,l\,N_A. \qquad \text{[S3]}$$

For an insulin monomer concentration of 1 mg/mL at 65° C, Eq. **S3** results in $\Delta G_r^\circ = -25.6$ kJ · mol^{-1}, where N_A is the Avogadro constant. This magnitude of change in free energy is of the same order of magnitude as previously reported for insulin (4). Considering the sources of error in the calculation, this estimate is in fair agreement with previous reports.

Power Density and Surface Stress

The power density, PD, is given by the power (P)-to-mass (m_P) ratio as follows:

$$PD = P/m_P. \qquad \text{[S4]}$$

The maximal power generated by the growth of bovine insulin spherulites was calculated from the stall force, number of fibrils, N_f, and the measured rate of cantilever deflection, v:

$$P = FN_f v. \qquad \text{[S5]}$$

The deflection of the cantilever tip, δ, area of the cantilever face, A, and density of the spherulite, ρ_S, were used to find the mass of the growing amyloid fibrils:

$$m_P = \delta A \rho_S. \qquad \text{[S6]}$$

The power density for the growing spherulite amyloid clusters was found to be 1.24 ± 0.52 mW/kg. As the insulin spherulites investigated consist of over 90% liquid, it is conceivable that the power density for pure amyloid material could be up to an order of magnitude higher than the value reported here.

The difference interfacial stress acting on the cantilevers, the surface stress $\Delta\sigma$, was determined by applying Stoney's equation as previously reported for chemical actuators (5):

$$\Delta\sigma = \frac{Et^2}{3(1-\nu)h^2}\delta, \qquad \text{[S7]}$$

where E is the Young's modulus of PDMS, 1 MPa, ν is the Poisson's ratio of 0.49, and h and t are the length and thickness of the cantilever. For the growing insulin spherulites, this resulted in a range of $\Delta\sigma$ of 0.8–2.3 N·m^{-1}.

1. Footer MJ, Kerssemakers JWJ, Theriot JA, Dogterom M (2007) Direct measurement of force generation by actin filament polymerization using an optical trap. *Proc Natl Acad Sci USA* 104(7):2181–2186.
2. Theriot JA (2000) The polymerization motor. *Traffic* 1(1):19–28.
3. Smith MI, Foderà V, Sharp JS, Roberts CJ, Donald AM (2012) Factors affecting the formation of insulin amyloid spherulites. *Colloids Surf B Biointerfaces* 89:216–222.
4. Baldwin AJ, et al. (2011) Metastability of native proteins and the phenomenon of amyloid formation. *J Am Chem Soc* 133(36):14160–14163.
5. Zhou F, Shu W, Welland ME, Huck WTS (2006) Highly reversible and multi-stage cantilever actuation driven by polyelectrolyte brushes. *J Am Chem Soc* 128(16): 5326–5327.

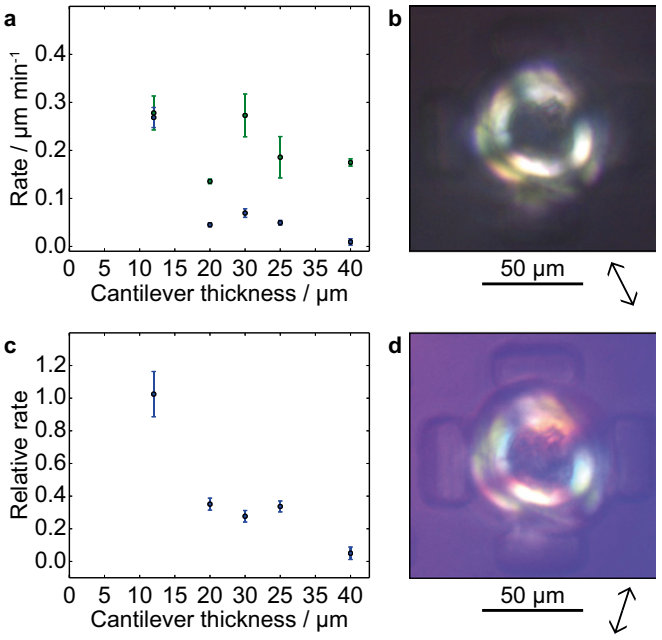

Fig. S1. Spherulite growth kinetics. (*A*) The measured rates of spherulite growth (green) and cantilever deflection (blue) against *t*; error bars show the SEM. (*B*) Spherulite, after growth between 20-μm cantilevers, placed between crossed polarizers and a wave plate at 90°. (*C*) The relative rates of cantilever deflection to spherulite growth; error bars represent the SEM. (*D*) Spherulite placed between crossed polarizers and a wave plate at 45°.

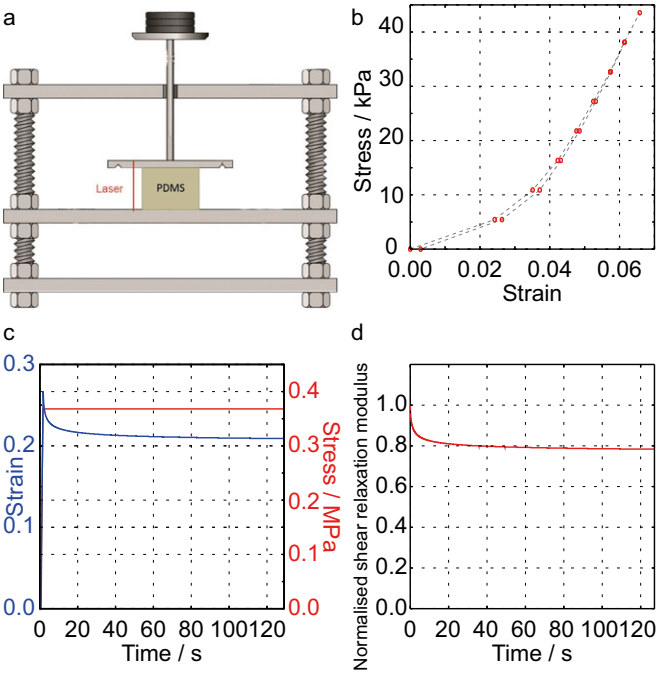

Fig. S2. Material properties of PDMS. (*A*) Diagram illustrating the setup for the compression tests. (*B*) Stress/strain measurement from compression test of PDMS. This shows nonlinear hyperelastic behavior. (*C*) Relaxation test of the PDMS; the left vertical axis shows the strain, and the right vertical axis the stress, both against time. (*D*) The normalized shear relaxation modulus against time.

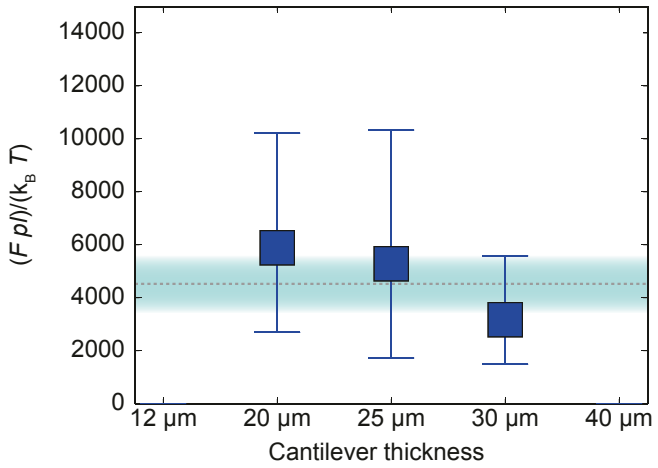

Fig. S3. Dimensionless force. The stall force per fibril scaled by the polymer length, Boltzmann constant, and absolute temperature, shown for each cantilever thickness.

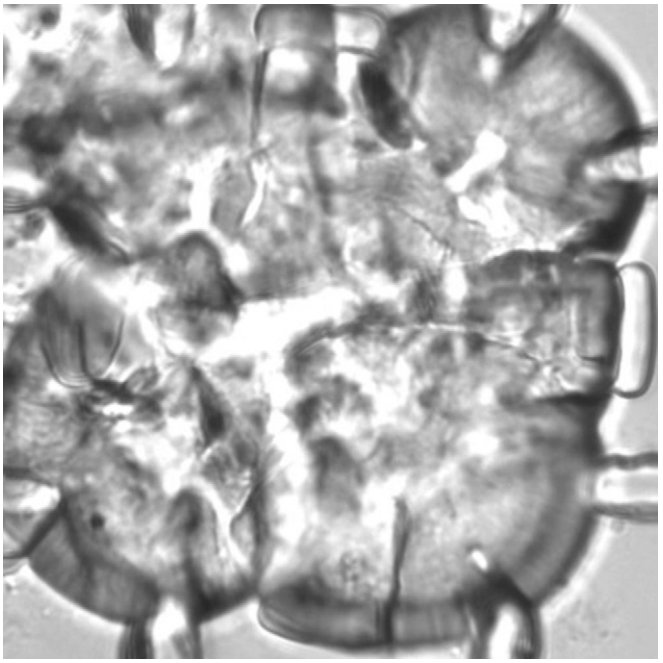

Movie S1. Video of images recorded for a growing spherulite between microcantilevers with a depth of 12 μm; for these cantilevers, no stall point was observed. Images were recorded at 30-s intervals.

Movie S1

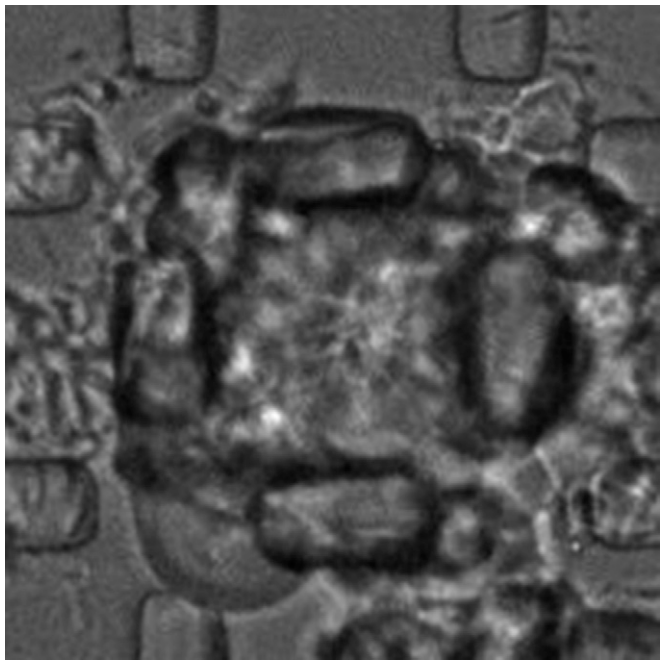

Movie S2. Video of images recorded for a growing spherulite between microcantilevers with a depth of 20 μm; for these cantilevers, a stall point was observed. Images were recorded at 30-s intervals.

Movie S2

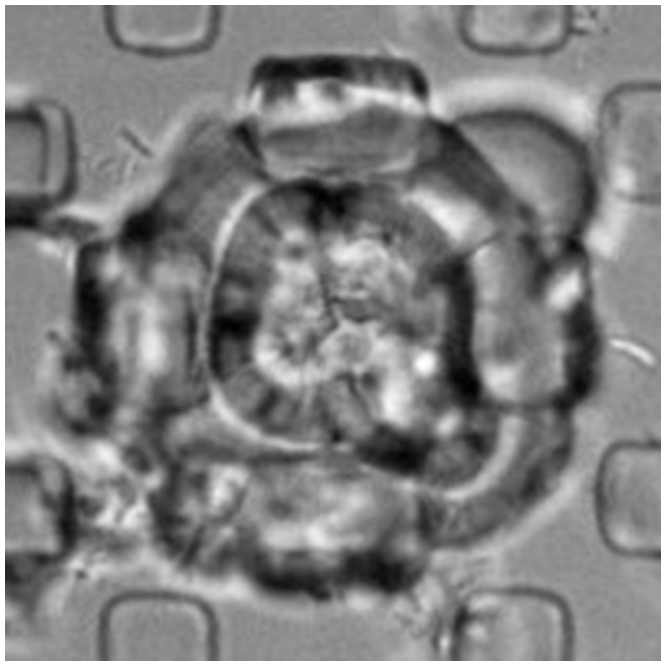

Movie S3. Video of images recorded for a growing spherulite between microcantilevers with a depth of 25 μm; for these cantilevers, a stall point was observed. Images were recorded at 30-s intervals.

Movie S3

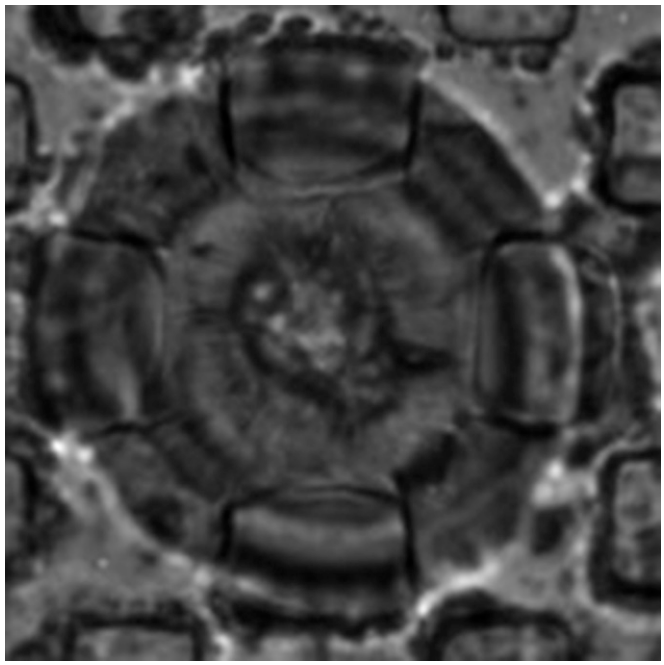

Movie S4. Video of images recorded for a growing spherulite between microcantilevers with a depth of 30 μm; for these cantilevers, a stall point was observed. Images were recorded at 30-s intervals.

Movie S4

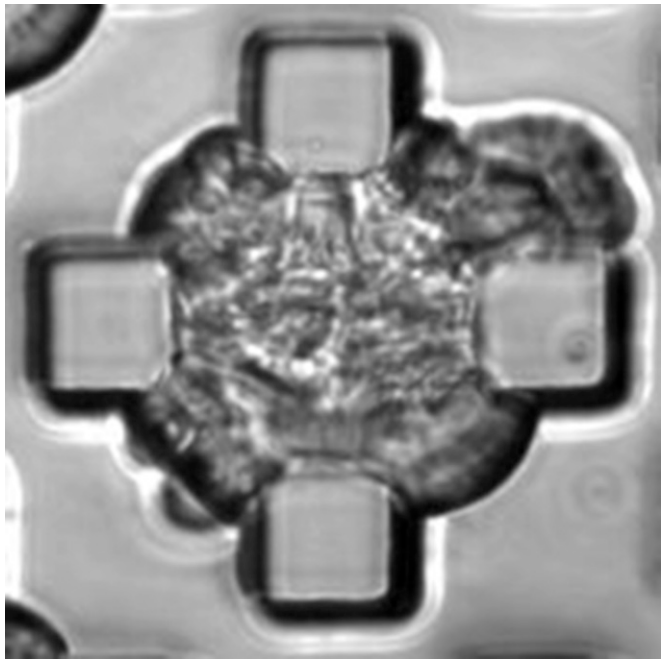

Movie S5. Video of images recorded for a growing spherulite between microcantilevers with a depth of 40 μm; no deflection was observed for these cantilevers. Images were recorded at 30-s intervals.

Movie S5

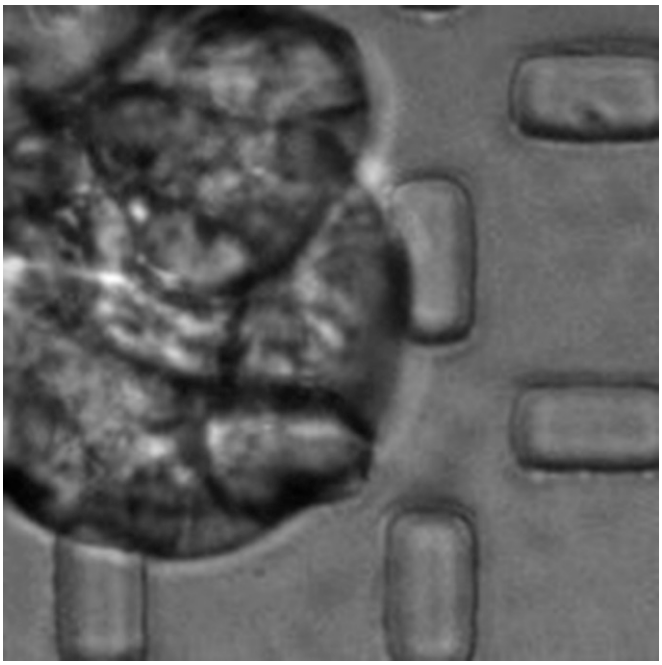

Movie S6. Video of images recorded for a group of spherulites where the monomer supply has been stopped. The images were recorded at 30-s intervals and show a period of 4 h.

Movie S6